

# Real-Time Observation of Nonclassical Protein Crystallization Kinetics

Andrea Sauter,<sup>†</sup> Felix Roosen-Runge,<sup>‡</sup> Fajun Zhang,<sup>\*,†</sup> Gudrun Lotze,<sup>||</sup> Robert M. J. Jacobs,<sup>§</sup> and Frank Schreiber<sup>†</sup>

<sup>†</sup>Institut für Angewandte Physik, Universität Tübingen, Auf der Morgenstelle 10, 72076 Tübingen, Germany

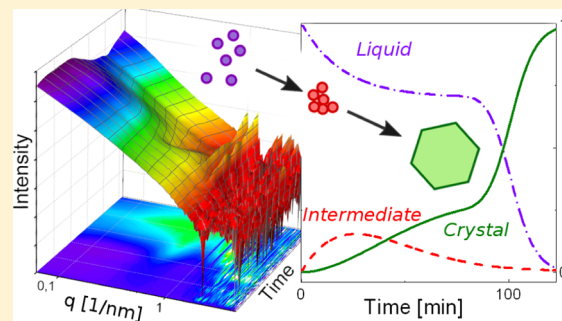
<sup>‡</sup>Institut Laue-Langevin, 71 avenue des Martyrs, 38042 Grenoble Cedex 9, France

<sup>||</sup>European Synchrotron Radiation Facility, 71 avenue des Martyrs, 38043 Grenoble Cedex 9, France

<sup>§</sup>Department of Chemistry, Chemistry Research Laboratory, University of Oxford, Mansfield Road, Oxford, OX1 3TA, United Kingdom

## Supporting Information

**ABSTRACT:** We present a real-time study of protein crystallization of bovine  $\beta$ -lactoglobulin in the presence of  $\text{CdCl}_2$  using small-angle X-ray scattering and optical microscopy. From observing the crystallization kinetics, we propose the following multistep crystallization mechanism that is consistent with our data. In the first step, an intermediate phase is formed, followed by the nucleation of crystals within the intermediate phase. During this period, the number of crystals increases with time, but the crystal growth is slowed down by the surrounding dense intermediate phase due to the low mobility. In the next step, the intermediate phase is consumed by nucleation and slow growth, and the crystals are exposed to the dilute phase. In this stage, the number of crystals becomes nearly constant, whereas the crystals grow rapidly due to access to the free protein molecules in the dilute phase. This real-time study not only provides evidence for a two-step nucleation process for protein crystallization but also elucidates the role and the structural signature of the metastable intermediate phase in this process.



## INTRODUCTION

Protein crystallization is the bottleneck of many projects in structural biology, since, in general, suitable crystallization conditions cannot be reliably predicted.<sup>1</sup> In classical nucleation theory, the solute molecules reversibly aggregate in the supersaturated solution and form nuclei with the density and structure of the crystals in the final stage. While classical nucleation theory has been successfully used in many systems, including protein crystallization under certain conditions,<sup>2</sup> various studies in the crystallization of proteins, colloids, and clathrate hydrates as well as biominerization have shown features beyond the classical view in the early stage of nucleation.<sup>3–8</sup>

In contrast to atomic systems, proteins and colloids often have an attractive interaction short-ranged compared to the size of the particles, as demonstrated by experiments,<sup>9–14</sup> theory,<sup>15,16</sup> and simulations.<sup>17,18</sup> Such short-ranged attraction leads to a liquid–liquid phase separation (LLPS) which is metastable with respect to the crystalline phase.<sup>18–22</sup> For these systems, a two-step (or multistep) mechanism of crystal nucleation has been discussed, i.e., an intermediate state, either cluster, aggregates, or a dense liquid phase, exists between the initial solution and the final crystalline state and may serve as the nucleation precursor. We note that throughout this paper,

we use the term ‘aggregates’ instead of ‘clusters’ to avoid misinterpretation. An important theoretical prediction is that nucleation is favored in the dense liquid intermediate phase compared to the dilute phase, since the surface energy of the dense phase is closer to the final crystalline state, and the free energy barrier for nucleation is lower.<sup>8,18,19</sup> However, experimental observations in several protein systems suggest that crystals nucleate mainly from the dilute phase or at the interface of the dense liquid droplets and grow outside of it into the dilute phase<sup>13,14,23</sup> Despite the existing various theoretical concepts, clear experimental evidence and suitable methods to distinguish the early stage of nucleation are rather rare.<sup>24–27</sup> Early studies of protein crystal growth in real space using atomic force microscopy have revealed many important features of the metastable protein clusters and their role in the nucleation process.<sup>27–31</sup> However, the quantitative real-time *in situ* characterization of the transition kinetics and microscopic structure from the metastable intermediate phase to the stable crystalline phase is still a challenge.

Our previous studies have shown that trivalent salts such as  $\text{YCl}_3$  lead to a reentrant condensation and metastable liquid–

Received: October 14, 2014

Published: January 8, 2015

liquid phase separation phase behavior in many solutions of negatively charged proteins.<sup>32–35</sup> Importantly, crystal growth depends on the exact location in the phase diagram: Depending on external control parameters such as salt concentration and temperature, classical crystallization or a temperature-dependent nonclassical process was observed but could not be analyzed in further detail regarding kinetics and nucleation mechanism. The optimum crystallization conditions were found close to the reentrant condensation phase boundaries.<sup>34</sup>

In this work, we investigate the crystallization *kinetics* of the globular protein  $\beta$ -lactoglobulin (BLG) in the presence of the divalent salt  $\text{CdCl}_2$  by real-time SAXS and optical microscopy. BLG has turned out to be a good model system for crystallization by tuning the protein interactions utilizing reentrant condensation with trivalent salts. Here, we focus on the effect of the formation of aggregates on the crystallization process and which crystallization pathways are followed. In a distinct phase diagram region, protein aggregates form before crystallization. Given the dimensions of proteins, a direct optical visualization of the nucleation process in protein solutions is not possible. Here, we employ the method of real-time SAXS, monitoring the nucleation process by means of structural information on the solutes such as protein monomers, crystals, and intermediates. These experiments raise interesting questions regarding protein nucleation. A model is proposed to explain the main features of the experiments. Different scenarios of crystal formation can be compared to the kinetic data. While the classical one-step nucleation describes the direct nucleation and growth from a homogeneous solution, in particular two nonconventional pathways are discussed (see Figure 1): first, a parallel process

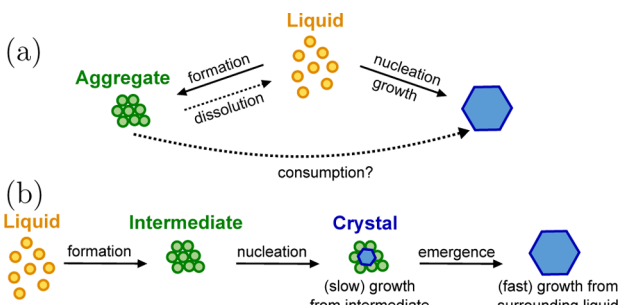


**Figure 1.** Schematic of all processes in two possible pathways of crystallization. (a) Nucleation directly from the liquid, parallel formation of “intermediates” that are redissolved or consumed by the growing crystals. (b) Intermediates are formed first and act as precursor for crystal nucleation.

of one-step crystal nucleation accompanied by an “intermediate” that forms and dissolves in the solution depending on concentration (Figure 1a). In this pathway, crystal growth takes place via the liquid or possibly by incorporation of aggregates, which, however, are not essential for crystal nucleation. Second, a two-step process of crystal nucleation within an intermediate that forms first from solution and is later transformed to crystals (Figure 1b).

## ■ EXPERIMENTAL SECTION

Lyophilized protein powder of BLG from bovine milk and the divalent salt cadmium chloride ( $\text{CdCl}_2$ ) were purchased from Sigma-Aldrich (product no. L3908 and 202908) and used as received.

Stock solutions were prepared by dissolving the protein powder or salt in deionized ( $18.2 \text{ M}\Omega$ ) and degassed Millipore water. All samples were prepared by mixing the needed amount of protein, salt stock solution, and Millipore water. The protein concentration was determined by UV absorption using an extinction coefficient of  $0.96 \text{ mL}\cdot\text{mg}^{-1} \text{ cm}^{-1}$  at a wavelength of  $278 \text{ nm}$ .<sup>36</sup> To avoid the effect of buffer on the phase behavior, no additional buffer was used for sample preparation. The pH of the solutions was monitored using a Seven Easy pH instrument from Mettler Toledo and was in between 6.0 and 7.0. Compared with the  $pI = 5.2$  of BLG,<sup>37</sup> the pH effect of added salt could not lead to the charge inversion of proteins.<sup>33,38</sup> All experiments were performed at 293 K.

Circular dichroism (J-720 spectrophotometer from Jasco Inc.) and Fourier transform infrared spectroscopy (FTIR) (IFS 48 from Bruker) were applied to monitor the stability of the protein secondary structure under the experimental conditions.

Crystal growth was followed by optical microscopy (DME from Leica Microsystem GmbH or AxioScope A1 from Zeiss). Before crystallization, protein stock solutions were filtered ( $100 \mu\text{m}$ ). The crystallization process was performed using either a vapor diffusion hanging drop method or a batch method between two narrow glass slides (thickness approximately  $300 \mu\text{m}$ ), sealed by silicone. Both methods gave similar results.

SAXS measurements were carried out at the ESRF, Grenoble, France at beamline ID02. With a sample-to-detector distance of 2 m and an energy of 16047 eV, the accessed  $q$ -range was  $0.06\text{--}4.3 \text{ nm}^{-1}$ . Details of the beamline, data collection, and calibration can be found in ref 39. For time-resolved SAXS measurements, freshly prepared sample solutions in a quartz capillary were quickly transferred to the sample station and the measurement started about 2–3 min after mixing. SAXS data were collected every 2 to 5 min depending on the samples. The exposure time was 0.05 s. To check the consistency of the measurements, the sample was shifted vertically to different positions. This cycle was repeated every 2–5 min. Only the data from one position as a function of time was used for the data analysis shown below, but data from all positions are consistent with our analysis.

## ■ RESULTS

### Experimental Phase Diagram and Protein Stability.

To provide a basis for the kinetic studies, we first present the experimental phase diagram of BLG in the presence of  $\text{CdCl}_2$  (Figure 2). Upon adding  $\text{CdCl}_2$ , BLG solutions show a sharp transition  $c^*$  from a clear solution at low  $\text{CdCl}_2$  concentrations (regime I) to a turbid one with massive precipitates at higher  $\text{CdCl}_2$  concentrations (regime II). At further increased salt concentrations, the precipitates are gradually dissolved and the solution becomes less turbid, but not completely clear even for

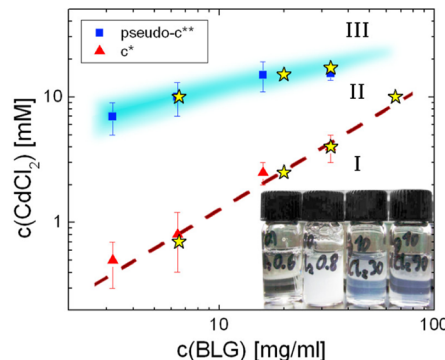


**Figure 2.** Experimental phase diagram of BLG and  $\text{CdCl}_2$  at room temperature. Yellow stars mark the conditions used for the SAXS experiments. Inset: Samples with a fixed BLG concentration ( $10 \text{ mg}/\text{mL}$ ) and increasing  $\text{CdCl}_2$  concentrations (from left to right:  $0.6, 0.8, 10, 30, 90 \text{ mM}$ ).

a very high salt concentration. This is in contrast to systems with trivalent salts where we observed a second border  $c^{**}$  above which samples become completely clear again (re-entrant effect).<sup>32,33</sup> We define this partial transition zone to clear solutions as pseudo- $c^{**}$ . The region above pseudo- $c^{**}$  is denoted as regime III. Zeta potential measurements show that a CdCl<sub>2</sub> concentration-dependent charge inversion of the protein takes place (SI, Figure S1b). In Figure 2, stars mark the conditions used for the real-time SAXS measurements. Under the current experimental conditions, no liquid–liquid phase separation was observed in BLG solutions in the presence of CdCl<sub>2</sub>, in contrast to some of the other protein-salt systems showing reentrant condensation.<sup>35</sup> In these cases, the liquid–liquid phase separation region is found as a closed area within the second regime.

We emphasize that the observed protein condensation is not caused by a change of the protein structure induced by CdCl<sub>2</sub>. We have performed Fourier transform infrared (FTIR) and circular dichroism spectroscopy for a broad protein and salt concentration range as presented in Figure 3. Both techniques

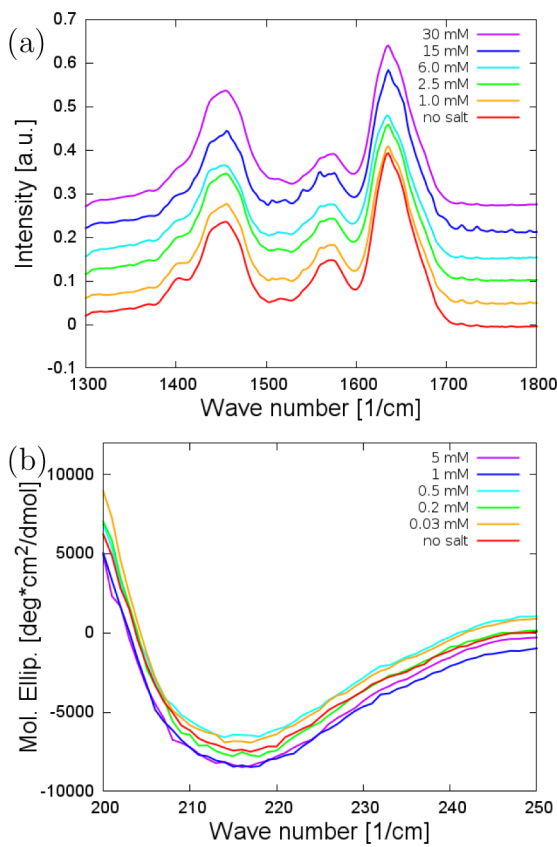


**Figure 3.** (a) FTIR results (amide I and II) for a BLG concentration of 20 mg/mL and CdCl<sub>2</sub> concentrations between 0 and 30 mM (covering all three regimes). (b) Circular dichroism spectra for samples with a BLG concentration of 0.2 mg/mL and CdCl<sub>2</sub> concentrations between 0 and 5 mM.

indicate no significant change on the secondary structure of the protein. Time-dependent FTIR spectra of the amide I and II bands also confirm that no significant structural change occurs during the entire crystallization process (SI, Figure S1a).

**Crystallization Followed by Optical Microscopy.** Crystallization of BLG in the presence of CdCl<sub>2</sub> was observed within a wide range of the above shown phase diagram. Slightly

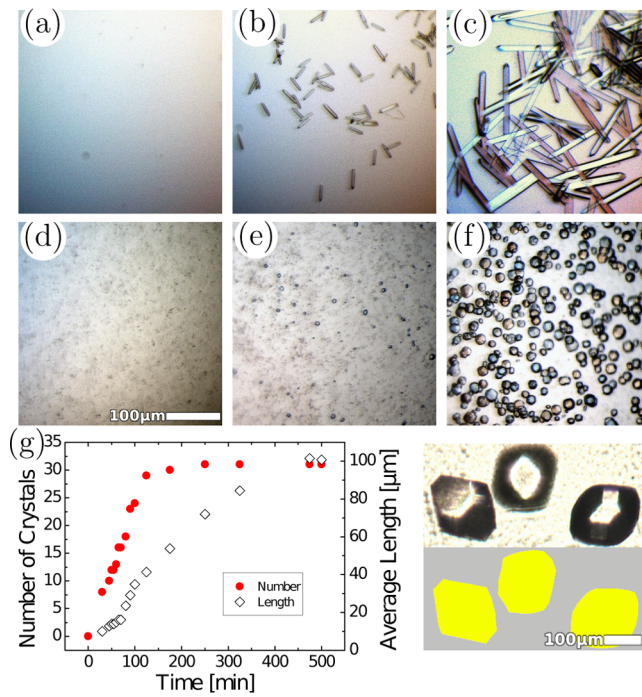


**Figure 4.** Real-time observation of crystal growth by optical microscopy. (a–c): Crystallization of a clear sample slightly below  $c^*$  (6.5 mg/mL BLG with 0.7 mM CdCl<sub>2</sub>), directly after preparation (a), after 30 min (b), and after several days (c). (d–f): Nonclassical crystallization in the pseudo- $c^{**}$  zone (3.3 mg/mL BLG with 7 mM CdCl<sub>2</sub>) 20 min (d), 30 min (e), and 120 min after preparation (f). (g): Quantitative analysis of a nonclassical crystallization process for a sample within pseudo- $c^{**}$  (20 mg/mL BLG with 15 mM CdCl<sub>2</sub>, see also SI Video S1). The number of crystals  $N$  (filled red circles, left axis) and the average length  $L = (A/N)^{1/2}$  (open diamonds, right axis) are plotted as a function of time. Right: Evaluation of the area  $A$  of crystals.

below and above  $c^*$ , no indications for a multistep process were observed: Crystals nucleate directly from a solution and grow larger without any visible clustering or liquid–liquid phase separation (Figure 4a–c). The typical shape of the crystals is needle-like under these conditions. In contrast, in the transition zone of pseudo- $c^{**}$  (Figure 4d–f), protein aggregates form quickly after sample preparation and the solution observed by optical microscopy becomes more turbid. During crystallization, the turbid solution becomes gradually clearer, indicating that the aggregates are consumed. Removing the aggregates by centrifuging can significantly reduce the number of crystals, as also shown in other protein systems.<sup>27</sup>

We further analyze the time dependence of the number and size of crystals. The visible area  $A$  of crystals in the microscopy pictures was determined by the open source program ImageJ.<sup>40</sup> The average crystal length can be estimated as  $L \approx (A/N)^{1/2}$ , where  $N$  is the number of crystals in the respective image. Figure 4g shows the evolution of  $L$  and  $N$  with time. In the beginning, the number of crystals increases linearly and then saturates. After the visible crystals stop increasing in number, they still significantly increase in size. The increase in  $L$  is slow until 80 min, then faster growth starts and eventually saturates due to depletion of protein. The effect of centrifuging on the number of crystals and the acceleration of the growth rate after 80 min suggest that nucleation is closely related to the amount of protein portioned in aggregates formed in the early stage of sample preparation.

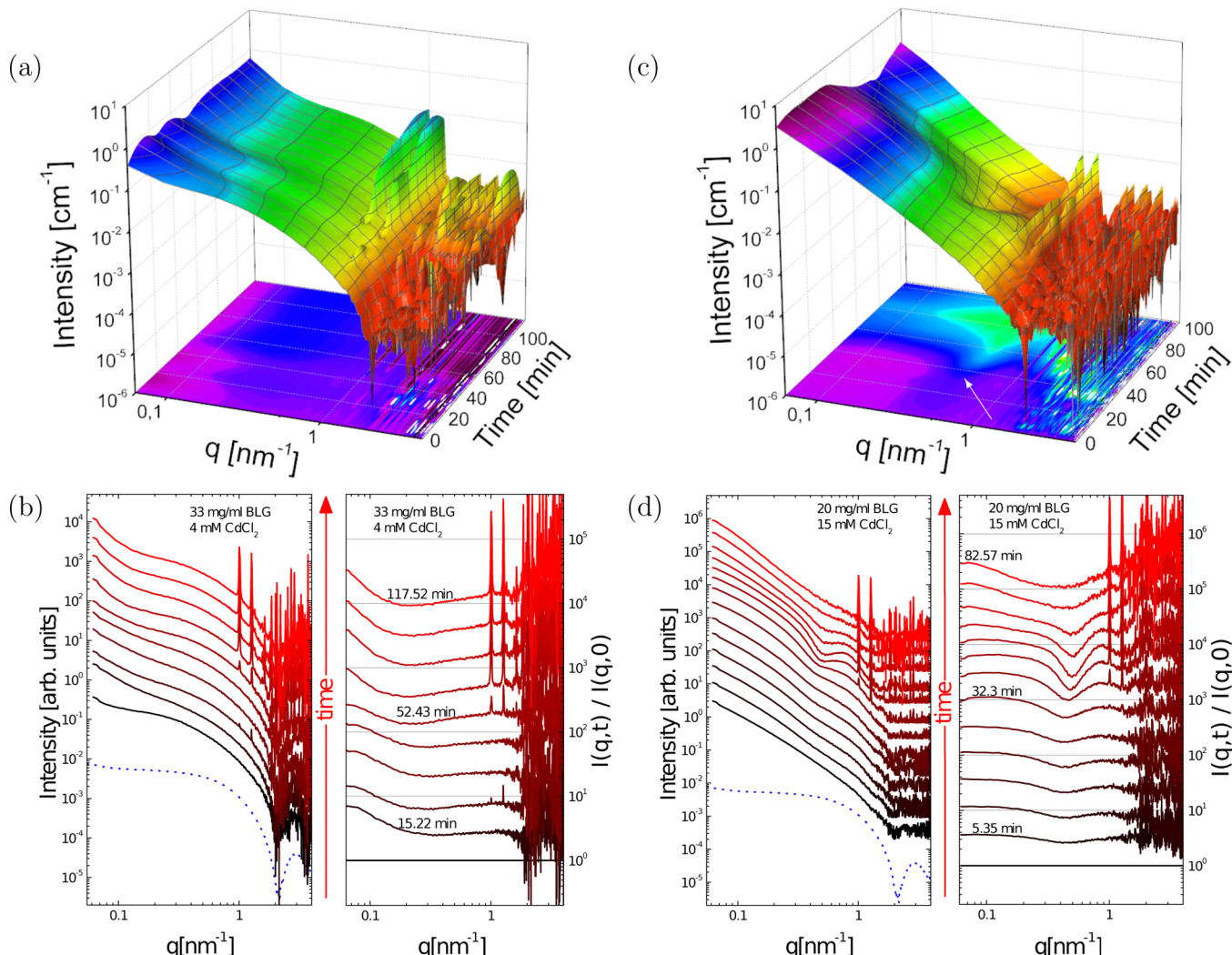


**Figure 5.** Real-time SAXS curves for 33 mg/mL BLG with 4 mM (a,b), i.e., slightly below  $c^*$ , and 20 mg/mL BLG with 15 mM CdCl<sub>2</sub> (c,d), i.e., within pseudo- $c^{**}$ . (a,c) 3D surface illustration of  $I(q, t)$ . The bottom projections are created from all curves divided by the first one. The arrow in (c) points to an additional structure forming before crystallization. (b,d) Single  $I(q, t)$  and  $I(q, t)/I(q, t = 0)$  curves at selective times multiplied by constant factors for better visibility. The blue dotted line shows the form factor of BLG at low concentrations.

**Crystal Growth Followed by Real-Time SAXS.** Because of the fast crystallization process and limited resolution of optical microscopy, it is impossible to deduce the role of protein aggregates on the nucleation process by this method. For this purpose, we employ real-time SAXS to follow the early stage of crystallization. Figure 5 shows time-resolved SAXS data for crystallization slightly below  $c^*$  (Figure 5a) and within the transition zone of pseudo- $c^{**}$  (Figure 5c). By dividing each curve by the first one, we monitor the evolution of the samples. This is shown in the bottom projections of the 3D-plots. In Figure 5b,d,  $I(q, t)$  and  $I(q, t)/I(q, t = 0)$  are plotted at selective times for further discussion. For comparison, the form factor of BLG is also shown (blue dotted line).

Below  $c^*$ , the scattering curves change gradually with time. After an induction time (20 min in the example shown in Figure 5a,b), Bragg peaks appear and grow with time. Less pronounced Bragg peaks at later times are caused by crystals sedimenting out of the beam position. This is occasionally observed close to  $c^*$ , where the samples are less viscous than within the pseudo- $c^{**}$  zone. Apart from that, the underlying shape of the curves barely changes with time. No indication of states other than solution and crystal was found. Similar

behavior was found for other samples slightly below and above  $c^*$ . Hence, close to  $c^*$ , the crystallization process is consistent with the observation by optical microscopy and can be explained by classical nucleation theory.

Importantly, within the region of pseudo- $c^{**}$ ,  $I(q, t)$  follows a power law of  $q^{-2}$  at low  $q$  directly after preparation (the change of the exponent is shown in Figure S2 in SI), deviating strongly from the form factor of BLG under physiological conditions (blue dotted line in Figure 5b,d). This is consistent with the formation of aggregates after sample preparation.<sup>41,42</sup> The data were analyzed by normalizing the time-dependent  $I(q, t)$  by  $I(q, t = 0)$ , which minimizes the effect of the form factor and the aggregate formation in the system and emphasizes the time-dependent relative changes. With increasing time, a broad maximum at 0.7–1.4 nm<sup>-1</sup> appears (Figure 5c,d). Since scattering probes molecular and solution structures directly and thus is sensitive to changes of particle correlations, the time-dependent change of this broad peak can be interpreted as the evolution of a new structural feature within the larger aggregates at length scales of about 10 nm. Over time, this broad peak increases in intensity until Bragg peaks start to be observed. The two most pronounced Bragg peaks located at

1.01 and 1.27 nm<sup>-1</sup> overlap with the broad maximum. The intensity of the Bragg peaks increases with time, whereas the broad peak shrinks and eventually disappears. Similar crystallization behavior was also observed for other samples within the region of pseudo- $c^*$  (cf. Figure 2).

To quantify the relationship between the aggregates (broad peak) and crystals (Bragg peaks) as a function of time, we use the concept of the degree of crystallinity known from semicrystalline polymers<sup>43</sup> for further data analysis: The intensity at the minimum (at around 0.5 nm<sup>-1</sup>) was subtracted to set  $I_{\min}$  to zero. Then, the broad peak in  $I(q, t)/I(q, t = 0)$  was fitted by a broad scaled Gaussian, and the remaining Bragg peaks were fitted by two further (sharp) Gaussian functions (Figure 6a). For different times, the enveloped area of the

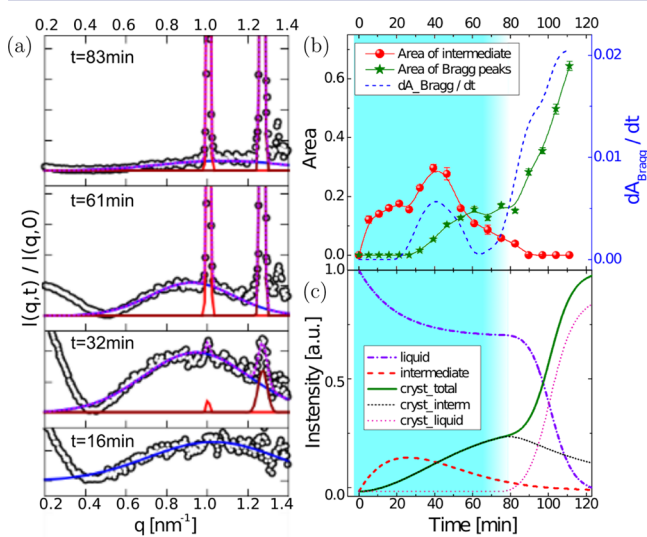


**Figure 6.** Analysis of the time-dependent data. (a) For data analysis, the areas of the intermediate and crystalline part of  $I(q, t)/I(q, t = 0)$  were evaluated. (b) Red spheres (left axis) show  $A_{\text{interm}}(t)$ , the integral of the broad Gaussian function, connected to the intermediate state from 0.4 to 1.3 nm<sup>-1</sup>. Green stars (left axis) show  $A_{\text{Bragg}}(t)$ , the integral of the two Bragg peaks in this area. The blue dashed line (right axis) shows the time derivative of  $A_{\text{Bragg}}(t)$ , the crystallization rate. The growth rate has a local maximum at the total maximum of  $A_{\text{interm}}(t)$ . (c) A rate equation model based on physically meaningful processes reproduces the experimental kinetic features. The light-cyan area marks the nucleation-dominated regime and is followed by the growth-dominated regime (no sharp transition).

broad region,  $A_{\text{interm}}$ , and the area of the Bragg peaks,  $A_{\text{Bragg}}$ , were followed over time, monitoring the crystallization kinetics.

Figure 6b shows  $A_{\text{interm}}$  (red spheres) and  $A_{\text{Bragg}}$  (green stars) as a function of time. The formation of the intermediate phase starts from the very first measurements on, increasing with time up to a maximum after approximately 42 min. Afterwards,  $A_{\text{interm}}$  decays gradually to zero.  $A_{\text{Bragg}}$ , on the other hand, is zero in the beginning and becomes visible after 30 min. Interestingly, the increase with time is nontrivial: After reaching a plateau around 50–80 min,  $A_{\text{Bragg}}$  increases dramatically. For further understanding, we show the first time derivative of  $A_{\text{Bragg}}$  which represents the crystallization rate (blue dashed line in Figure 6b, right axis), calculated at each point in time from the average of the incoming and outgoing slope. Interestingly,  $dA_{\text{Bragg}}/dt$  has a local maximum corresponding to the maximum of  $A_{\text{interm}}$ , suggesting that the crystallization rate is proportional to the amount of protein in these aggregates. Recalling the

observation in Figure 4g, the early stage of crystallization can be interpreted as dominated by the nucleation events. This suggests that nucleation occurs within the intermediate phase. The strong increase in  $A_{\text{Bragg}}$  after 80 min can be related to the growth-dominated stage as observed in Figure 4g. The same behavior could be observed for other conditions within the region of pseudo- $c^*$  followed by real-time SAXS. An analysis for a sample with 33 mg/mL BLG with 17 mM CdCl<sub>2</sub> can be found in the SI, Figures S3–5. In contrast, all tested conditions close to  $c^*$  show no signs of the existence of an intermediate phase between the initial solution and the final crystalline state.

**Discussion: Parallel One-Step Processes versus Two-Step Process.** Based on the above presented real-time results from both optical microscopy and SAXS, we suggest the following crystallization mechanism: In the first step, protein aggregates form as an intermediate and crystals nucleate from the aggregate precursor after a short induction time. The nucleation rate is thus proportional to the amount of the intermediate phase; as expected for such a two-step nucleation, a local maximum in the crystallization rate (and hence a point of inflection in  $A_{\text{Bragg}}$ ) occurs when  $A_{\text{interm}}$  is at its maximum. Crystal growth is slow, possibly due to the slow dynamics of molecules within the aggregates, which makes it difficult for proteins to diffuse to the growth front. However, such slow dynamics may be sufficient for nucleation as less molecules are involved in this process. We note that if the intermediate is in a kinetically arrested states (even slower dynamics), nucleation can be strongly impeded.<sup>19</sup> In the second step, the intermediate phase is consumed by nucleation and crystal growth, and the crystals grow rapidly by consuming free protein from the dilute phase. Proteins in the dilute phase (also in small aggregates as indicated from SAXS profiles and earlier studies<sup>44</sup>) can be easily incorporated into the crystal lattice. Importantly, the nucleation rate in the second step is significantly reduced, which further demonstrates the likely role of the protein aggregates as the precursor of a two-step nucleation process. All observations are explained very naturally using the two-step nucleation pathway based on clearly defined physical concepts (Figure 1b).

The proposed two-step nucleation mechanism can be further supported by using a rate equation model. Before looking into different quantitative models of the nucleation process, we note three qualitative model-free aspects directly from the data: (a) The intermediate forms very fast, while the initial crystal nucleation and growth are much slower. (b) Given the fast formation of intermediate, the disappearance of the intermediate has implications for its nature. At the time of disappearance, a considerable concentration in the liquid phase is still present, since the crystal growth is taking place even later. Thus, the intermediate is not in equilibrium with the liquid phase, but rather supplied by an excess concentration in the supersaturated liquid. (c) The plateau in the crystal formation indicates that the initial crystal growth is much slower than the final crystal growth.

One possible scenario involving an intermediate and crystals is a picture of two parallel one-step processes as sketched in Figure 1a. The intermediate would form from the supersaturated solution, and subsequently dissolve again, once the liquid phase is depleted by crystal nucleation and growth. While this scenario is consistent with observation (a) and (b) above, it cannot explain the plateau (c). Given the fast kinetics of the formation of the intermediate (a), the concentration in the liquid stays rather constant at the saturation concentration (b). Thus, once crystals are present, crystal growth should occur

with a similar steeply increasing signature as in the late growth state, instead of being stagnant for some period. Thus, the parallel picture fails to explain an essential aspect observed in the experiment.

We note that it may be possible to introduce *ad hoc* technical modifications of the one-step parallel scenario to force-fit the data. Note that these modifications necessarily would violate a picture of a one-step process along classical nucleation theory, and rather suggest an effective multistep process. We also note that the existence of heterogeneous nucleation or the combination of heterogeneous and homogeneous nucleation processes might lead to an overall growth kinetics similar to two or multiple parallel nucleation process, which again will not explain the plateau. Furthermore, these modifications would rely on a certain combination of parallel one-step processes, which makes the consequential two-step mechanism more feasible to explain the experimental results.

The second scenario is the picture of a two-step process of crystal nucleation from a previously formed intermediate as represented by Figure 1b. As shown in Figure 6c, a related model of rate equations based on processes with a clear physical meaning reproduces all features with very good agreement with the data. In the following, the system is described in terms of the mass fractions of protein in the liquid solution ( $L$ ), in the intermediate phase ( $I$ ) and within crystals in the solution ( $C_L$ ) and intermediate phase ( $C_I$ );  $(x)_+$  equals  $x$  for positive  $x$  and 0 otherwise.

First, the intermediate forms from the solution until the liquid solution reaches a stable mass fraction  $L_0$ :  $\Delta_I = k_I(L - L_0)_+$ . Second, crystals nucleate slowly from the intermediate:  $\Delta_n = k_n I$ . Third, the crystal growth within the intermediate depends on the amount of crystals and intermediate:  $\Delta_{gI} = k_{gI} C_I$ . Fourth, once the intermediate phase is consumed and falls below a certain volume per crystal, the crystals become exposed to the liquid phase:  $\Delta_t = k_t C_I (\alpha_t C_I - I)_+$ .  $\alpha_t$  is the ratio of the critical intermediate volume per crystal volume. Finally, once crystals emerged into the liquid phase, the crystal growth in the liquid phase consumes the free protein molecules:  $\Delta_{gL} = k_{gL} L C_L$ .

Consequently, the rate equations read

$$\partial_t L = -\Delta_I - \Delta_{gL} \quad (1)$$

$$\partial_t I = \Delta_I - \Delta_n - \Delta_{gI} \quad (2)$$

$$\partial_t C_I = \Delta_n - \Delta_t + \Delta_{gI} \quad (3)$$

$$\partial_t C_L = \Delta_e + \Delta_{gL} \quad (4)$$

with the initial conditions  $L(0) = 1$ ,  $I(0) = 0$ ,  $C_I(0) = 0$ , and  $C_L(0) = 0$ . The temporal evolution has been calculated with the Euler method using the following choices of model parameter:  $k_I = 0.05 \text{ min}^{-1}$ ,  $k_n = 0.02 \text{ min}^{-1}$ ,  $k_{gI} = 0.1 \text{ min}^{-1}$ ,  $k_{gL} = 0.2 \text{ min}^{-1}$ ,  $k_e = 1.0 \text{ min}^{-1}$ ,  $L_0 = 0.7$ , and  $\alpha_t = 0.2$ . Note that the absolute values of the rates are consistent with the physical picture of this work and all parameters take physically reasonable values. We emphasize that the general qualitative result is robust against slight changes of the absolute values.

## CONCLUSION

In summary, our real-time SAXS and optical microscopy study of protein BLG crystallization in the presence of  $\text{CdCl}_2$  provides evidence for a two-step nucleation mechanism, i.e., protein aggregates form first as an intermediate and crystals nucleate within these aggregate precursors after an induction

time. The nucleation rate is thus proportional to the amount of the intermediate phase, consistent with the appearance of a local maximum in the crystallization rate at the maximum quantity of the intermediate. However, the crystal growth rate is low, which might be due to the low mobility of proteins within the aggregates. This step lasts until the intermediate phase is consumed by crystallization, then crystal growth becomes faster as proteins in the dilute phase can diffuse to and incorporate into the growth front directly. In contrast, the nucleation rate is significantly reduced, which further demonstrates the role of the protein aggregates as the precursor of a two-step nucleation process. The experimental observations on the nonclassical growth kinetics have been interpreted using a rate equation model. In addition, these measurements demonstrate a noninvasive method to study *in situ* and in real-time the kinetics of nonclassical growth processes on nanometer length scales.

## ASSOCIATED CONTENT

### S Supporting Information

A video of the crystal growth, real-time FTIR spectra of the protein,  $\zeta$  potential measurements under the same conditions as the CD measurements, and an additional analyzed time-dependent SAXS study. This material is available free of charge via the Internet at <http://pubs.acs.org>.

## AUTHOR INFORMATION

### Corresponding Author

\*fajun.zhang@uni-tuebingen.de

### Notes

The authors declare no competing financial interest.

## ACKNOWLEDGMENTS

The authors thank the DFG for financial support and H.-J. Schöpe and M. Oettel for valuable discussions and comments. A.S. acknowledges a fellowship of the Landesgraduiertenförderung. A.S. thanks V. Niemann for the assistance in CD measurements and T. Stehle (IFIB, Universität Tübingen) for sharing their lab resources.

## REFERENCES

- Nanev, C. N. *Prog. Cryst. Growth Charact. Mater.* **2013**, *59*, 133–169.
- Sleutel, M.; Lutsko, J.; Van Driessche, A. E.; Durán-Olivencia, M. a.; Maes, D. *Nat. Commun.* **2014**, *5*, 5598.
- Jacobson, L. C.; Hujo, W.; Molinero, V. *J. Am. Chem. Soc.* **2010**, *132*, 11806–11.
- Cölfen, H.; Antonietti, M. *Mesocrystals and nonclassical crystallization*; John Wiley & Sons: West Sussex, 2008.
- Gebauer, D.; Völkel, A.; Cölfen, H. *Science* **2008**, *322*, 1819–22.
- Gebauer, D.; Kellermeier, M.; Gale, J. D.; Bergström, L.; Cölfen, H. *Chem. Soc. Rev.* **2014**, *43*, 2348–71.
- Wallace, A. F.; Hedges, L. O.; Fernandez-Martinez, A.; Raiteri, P.; Gale, J. D.; Waychunas, G. A.; Whitelam, S.; Banfield, J. F.; De Yoreo, J. J. *Science* **2013**, *341*, 885–889.
- Sear, R. P. *Int. Mater. Rev.* **2012**, *57*, 328–356.
- Gliko, O.; Neumaier, N.; Pan, W.; Haase, I.; Fischer, M.; Bacher, A.; Weinkauf, S.; Vekilov, P. G. *J. Am. Chem. Soc.* **2005**, *127*, 3433–3438.
- Gliko, O.; Pan, W.; Katsonis, P.; Neumaier, N.; Galkin, O.; Weinkauf, S.; Vekilov, P. G. *J. Phys. Chem. B* **2007**, *111*, 3106–3114.
- Pan, W.; Galkin, O.; Filobelo, L.; Nagel, R. L.; Vekilov, P. G. *Biophys. J.* **2007**, *92*, 267–277.

- (12) Pan, W.; Vekilov, P. G.; Lubchenko, V. *J. Phys. Chem. B* **2010**, *114*, 7620–30.
- (13) Chen, Q.; Vekilov, P. G.; Nagel, R. L.; Hirsch, R. E. *Biophys. J.* **2004**, *86*, 1702–1712.
- (14) Liu, Y.; Wang, X.; Ching, C. B. *Cryst. Growth Des.* **2010**, *10*, 548–558.
- (15) Hutchens, S. B.; Wang, Z.-G. *J. Chem. Phys.* **2007**, *127*, 084912.
- (16) Tóth, G. I.; Puszta, T.; Tegze, G.; Tóth, G.; Gránásy, L. *Phys. Rev. Lett.* **2011**, *107*, 175702.
- (17) Schilling, T.; Schöpe, H. J.; Oettel, M.; Opletal, G.; Snook, I. *Phys. Rev. Lett.* **2010**, *105*, 025701.
- (18) Wolde, P. R. t.; Frenkel, D. *Science* **1997**, *277*, 1975–1978.
- (19) Vekilov, P. G. *Cryst. Growth Des.* **2004**, *4*, 671–685.
- (20) Gunton, J.; Shirayev, A.; Pagan, D. *Protein Condensation: Kinetic Pathways to Crystallization and Disease*; Cambridge University Press: Cambridge, U.K., 2007.
- (21) Piazza, R. *Curr. Opin. Colloid Interface Sci.* **2000**, *5*, 38–43.
- (22) Anderson, V. J.; Lekkerkerker, H. N. W. *Nature* **2002**, *416*, 811–815.
- (23) Ray, W. J.; Bracker, C. *J. Cryst. Growth* **1986**, *76*, 562–576.
- (24) Schöpe, H. J.; Bryant, G.; van Megen, W. *Phys. Rev. Lett.* **2006**, *96*, 175701.
- (25) Zhang, T. H.; Liu, X. Y. *J. Am. Chem. Soc.* **2007**, *129*, 13520–13526.
- (26) Savage, J. R.; Dinsmore, A. D. *Phys. Rev. Lett.* **2009**, *102*, 198302.
- (27) Sleutel, M.; Van Driessche, A. E. S. *Proc. Nat. Sci. USA* **2014**, *111*, E546–E553.
- (28) Malkin, A. J.; Kuznetsov, Y. G.; Land, T.; DeYoreo, J. J.; McPherson, A. *Nat. Struct. Biol.* **1995**, *2*, 956–959.
- (29) Kuznetsov, Y.; Malkin, A.; McPherson, A. *Phys. Rev. B* **1998**, *58*, 6097–6103.
- (30) Mcpherson, A.; Malkin, A. J.; G, K. Y. *Annu. Rev. Biophys. Biomol. Struct.* **2000**, *29*, 361–410.
- (31) Van Driessche, A. E. S.; García-Ruiz, J. M.; Delgado-López, J. M.; Sazaki, G. *Cryst. Growth Des.* **2010**, *10*, 3909–3916.
- (32) Zhang, F.; Skoda, M. W. A.; Jacobs, R. M. J.; Zorn, S.; Martin, R. A.; Martin, C. M.; Clark, G. F.; Wegler, S.; Hildebrandt, A.; Kohlbacher, O.; Schreiber, F. *Phys. Rev. Lett.* **2008**, *101*, 148101.
- (33) Zhang, F.; Wegler, S.; Ziller, M. J.; Ianeselli, L.; Heck, B. S.; Hildebrandt, A.; Kohlbacher, O.; Skoda, M. W. A.; Jacobs, R. M. J.; Schreiber, F. *Proteins* **2010**, *78*, 3450–3457.
- (34) Zhang, F.; Zocher, G.; Sauter, A.; Stehle, T.; Schreiber, F. *J. Appl. Crystallogr.* **2011**, *44*, 755–762.
- (35) Zhang, F.; Roth, R.; Wolf, M.; Roosen-Runge, F.; Skoda, M. W. A.; Jacobs, R. M. J.; Sztucki, M.; Schreiber, F. *Soft Matter* **2012**, *8*, 1313–1316.
- (36) Sober, H. A. *CRC Handbook of Biochemistry: Selected data for molecular biology*; CRC: Boca Raton, FL, 1970.
- (37) Elofsson, U. M.; Paulsson, M. A.; Arnebrant, T. *Langmuir* **1997**, *13*, 1695–1700.
- (38) Roosen-Runge, F.; Heck, B. S.; Zhang, F.; Kohlbacher, O.; Schreiber, F. *J. Phys. Chem. B* **2013**, *117*, 5777–5787.
- (39) Narayanan, T. Chapter Synchrotron small-angle X-ray Scattering. In *Soft Matter Characterization*; Borsali, R., Pecora, R., Eds.; Springer: New York, 2008; p 899ff.
- (40) Schneider, C.; Rasband, W.; Eliceiri, K. *Nat. Methods* **2012**, *9*, 671–675.
- (41) Glatter, O.; Kratky, O. *Small angle X-ray scattering*; Academic Press: London, 1982.
- (42) Lindner, P.; Zemb, T. *Neutrons, X-rays, and Light: Scattering Methods Applied to Soft Condensed Matter*; Elsevier: Amsterdam, The Netherlands, 2002.
- (43) Strobl, G. *The physics of polymers*, 3rd ed.; Springer: Berlin, Germany, 2007; Chapter 5.
- (44) Zhang, F.; Roosen-Runge, F.; Sauter, A.; Roth, R.; Skoda, M. W. A.; Jacobs, R.; Sztucki, M.; Schreiber, F. *Faraday Discuss.* **2012**, *159*, 313–325.